MEDWIN PUBLISHERS
Committed to Create Value for Researchers

Nanomedicine & Nanotechnology Open Access
ISSN: 2574-187X

Novel Magnetic Levitation of Nanoiron Oxide for Dynamically Measuring Crystallinity and Uniformity

Zhong ZY, Huang YB, Wang YJ, Xiao ZR and Hsu C*

Department of Semiconductor Engineering, Longhua University of Science and Technology, Taiwan

***Corresponding author:** Chen Hsu, Department of Semiconductor Engineering, Longhua University of Science and Technology, Taiwan, Email: chenhsuemail@yahoo.com.tw

Research Article

Volume 8 Issue 4

Received Date: October 30, 2023

Published Date: November 14, 2023

DOI: 10.23880/nnoa-16000273

Abstract

This study explores the magnetic levitation (maglev) characteristics of superparamagnetic iron oxides (Fe_3O_4) used as motor-driven rotors in gyroscopes under low-alternating magnetism. Herein, superparamagnetic Fe_3O_4 was synthesized in a nanopowder form using the sol–gel method. The maglev force that stabilizes a rotating gyroscope depends on the rotation speed. This force exhibits a wide range of values. The stability of the synthesized superparamagnetic Fe_3O_4 increases with its size. The rotation stability was measured based on the size of a red laser spot and was found to depend on the rotation speed. Under a low magnetic field, superparamagnetic materials exhibit high stability. Herein, the superparamagnetic phase exhibits excellent stability. With increasing rotation speed, the superparamagnetic material exhibits strong magnetization. The nanoiron oxide is used to dynamically measure crystallinity and uniformity. Additionally, inversion recovery shows improved gyrostabilization for the superparamagnetic material.

Keywords: Magnetic Levitation; Superparamagnetic; Iron Oxide; Crystallinity; Uniformity

Abbreviations: SPMNPs: Superparamagnetic Nano particles; SEM: Scanning Electron Microscopy; XRD: X-ray Diffraction.

Introduction

Current-generation photolithography used in semiconductor manufacturing employs a magnetic levitation (maglev) stage for high-precision operations. This maglev stage uses a single, magnetically levitated moving part to provide fine six-degree-of-freedom motion control. This design results in an oscillator with a tunable resonance, which can be monitored in a nonlinear manner, necessitating nonlinear analyses of the energy potential of prototypical nonlinear systems [1-5].

The maglev stage has also been utilized in other high-precision motion applications, including for the transportation of rotor bearings. The utilization of the maglev stage is simpler than traditional approaches and offers a faster dynamic response and higher mechanical reliability. Noncontact bearings, flywheels, and momentum wheels are examples of such applications. Superparamagnetic nanoparticles (SPMNPs) have multimodal functionalities and tunable characteristics, making them suitable for application in various mechanical applications [6,7].

Biocell applications often employ a gyroscope comprising superparamagnetic iron oxide (Fe_3O_4) nanoparticles (SPIONs). Cells can be manipulated to obtain complex tissue structures, which are better than those achieved using conventional culture methods. This is achieved by strategically applying magnets and manipulating the properties of SPIONs using a remote magnetic field. Moreover, a nanoarchitecture can be constructed by attaching various chemical or biological molecules to the surface nanoparticles [8-10].

The levitation profiles of cells and cellular events exhibit characteristic patterns for different cell types (e.g., cancer, blood, bacteria, and yeast). The formation of ellipsoidal biomolecular bands can be attributed to levitated plasma biomolecules. These bands can be used to identify distinct differences in levitation and density profiles among various cancer cell lines as well as the heterogeneity within the seemingly homogeneous cell populations. These features have considerable clinical importance, especially for modeling diseases in plasma donors [10-11].

Materials and Methods

The material selected for this study was superparamagnetic Fe_3O_4. Its nanopowder form was fabricated using the sol–gel method. Initially a 0.08-M 100-mL NaOH solution was mixed with a 0.2-M 100-mL NaNO3 solution. This was followed by a slow addition of a 0.025-M 50-mL $FeSO_4$ solution. The resultant solution was heated at 90°C in a water bath for 4 h. Finally, the product was rinsed with deionized water and dried. Several characterization techniques, including scanning electron microscopy (SEM), X-ray diffraction (XRD), and maglev force measurements and magnetization, rotation stability, and inversion recovery experiments, were conducted.

Results and Discussion

A spinning coat was applied to an Al rotor. According to Lenz's law, the axis induced a change in the magnetic flux. The rotor compensated for this flux and the induced flux loss, while the axis hindered any increase in the flux. The corresponding force induces a downward force. A schematic is shown in Figure 1. In this schematic, four magnets were placed to create a magnetic field of nanoparaferromagnetic Fe_3O_4.

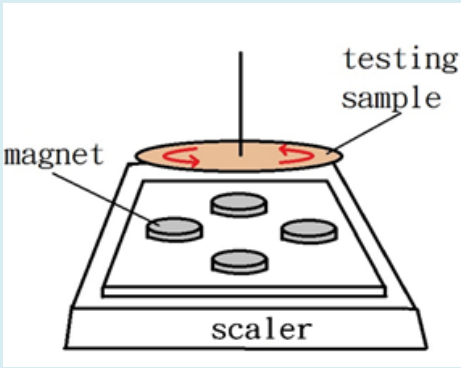

Figure 1: Schematic illustrating magnetic flux.

The tested material was secured on a spinning motor, with a magnet positioned below a scalar level of 2 cm. A red laser was projected onto the rotor surface and reflected onto the recorder paper. The rotor was subsequently spun at varying speeds, with values recorded from the scalar and measured in the projected area on the paper. The applied force acted on the motor-driven rotor, and its effects were recorded on video and used to calculate the recovery time. The factors affecting inversion recovery, including force action, inertia moment, and angular velocity, were recorded. The setup for a tachometer and red laser is shown in Figure 2.

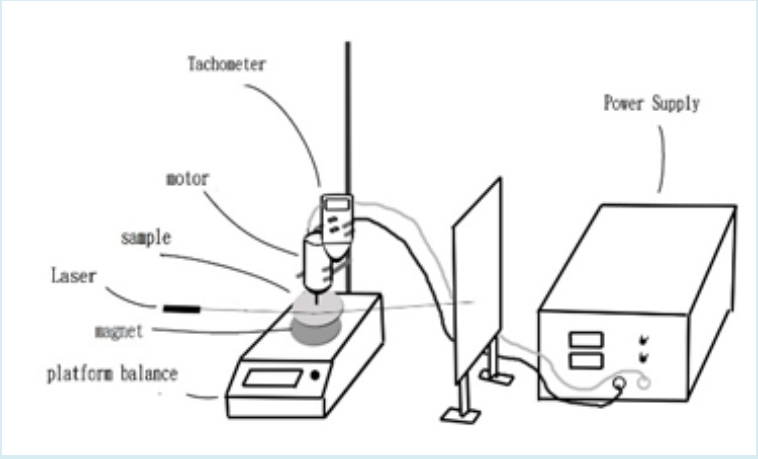

Figure 2: Experimental setup utilizing a tachometer and red laser for measuring magnetic levitation.

Fe_3O_4 nanoparticles were synthesized using the sol–gel method. The surface morphology of Fe_3O_4, observed through SEM, is presented in Figure 3a. The particle size is approximately 50 nm. The crystal structure, as analyzed

using XRD, shows a peak in the spectrum (Figure 3b), which matches with the JCPDS#01-075-0449 card, indicating that the crystal structure aligns well with the SPIONs.

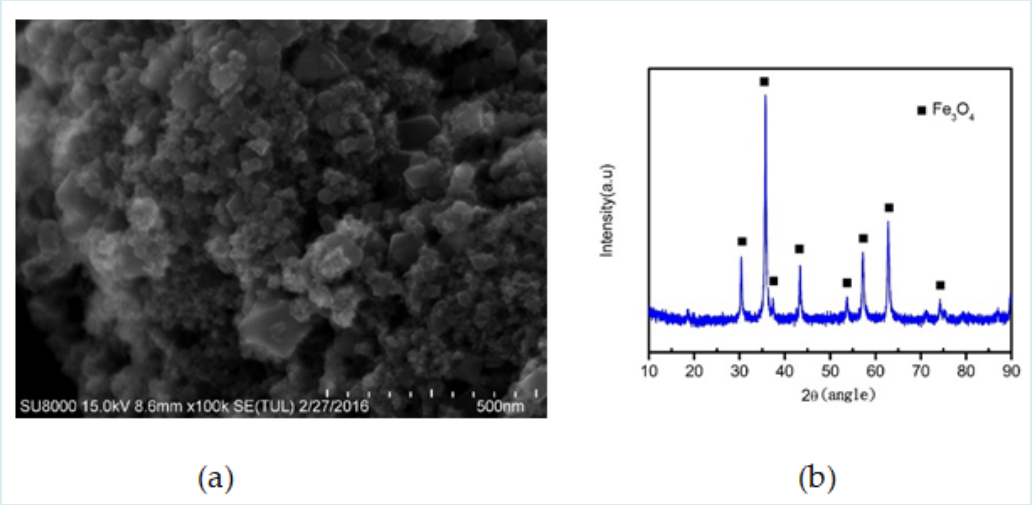

Figure 3: (a) Scanning electron microscopy image of superparamagnetic iron oxide nanoparticles and (b) the corresponding lattice structure analyzed using X-ray diffraction.

Magnetization corresponds to M = χ·H, where χ represents the magnetic susceptibility and H represents the magnetic strength. The variations of χ with rotation speed under magnetic fields of 46.0 and 140.6 mG are presented in Figure 4. At a low magnetic field of 46 mG, the susceptibility of the SPIONs increases with the increasing rotation speed. At a high magnetic field of 140.6 mG, all magnetic materials exhibit higher susceptibility than at a low magnetic field of 46.0 mG, with the SPIONs exhibiting the highest susceptibility.

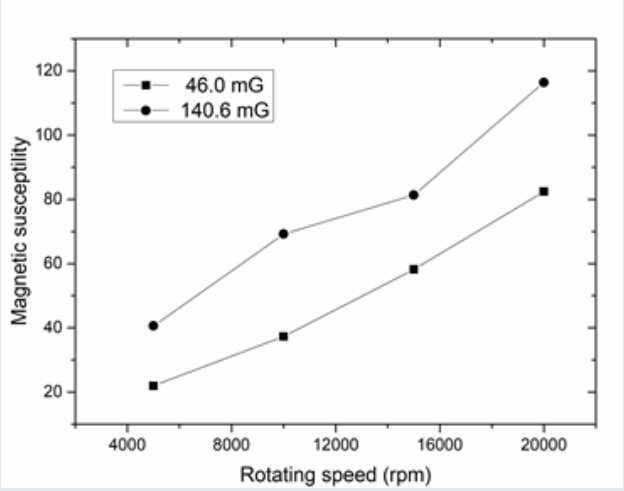

Figure 4: Magnetic susceptibilities under different magnetic fields.

The corresponding buoyancy of the SPIONs is depicted in Figure 5. At a low magnetic field of 46.0 mG, the buoyancy increases when the rotation speed exceeded 12,000 rpm. At a high magnetic field of 140.6 mG, superparamagnetic Fe_3O_4 exhibits a high buoyancy, which continued to increase with increasing rotation speed.

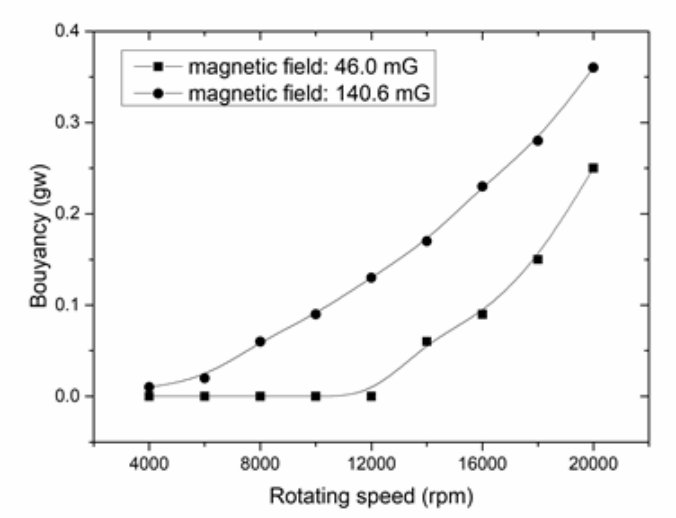

Figure 5: Variations in buoyancy with rotation speed under different magnetic fields.

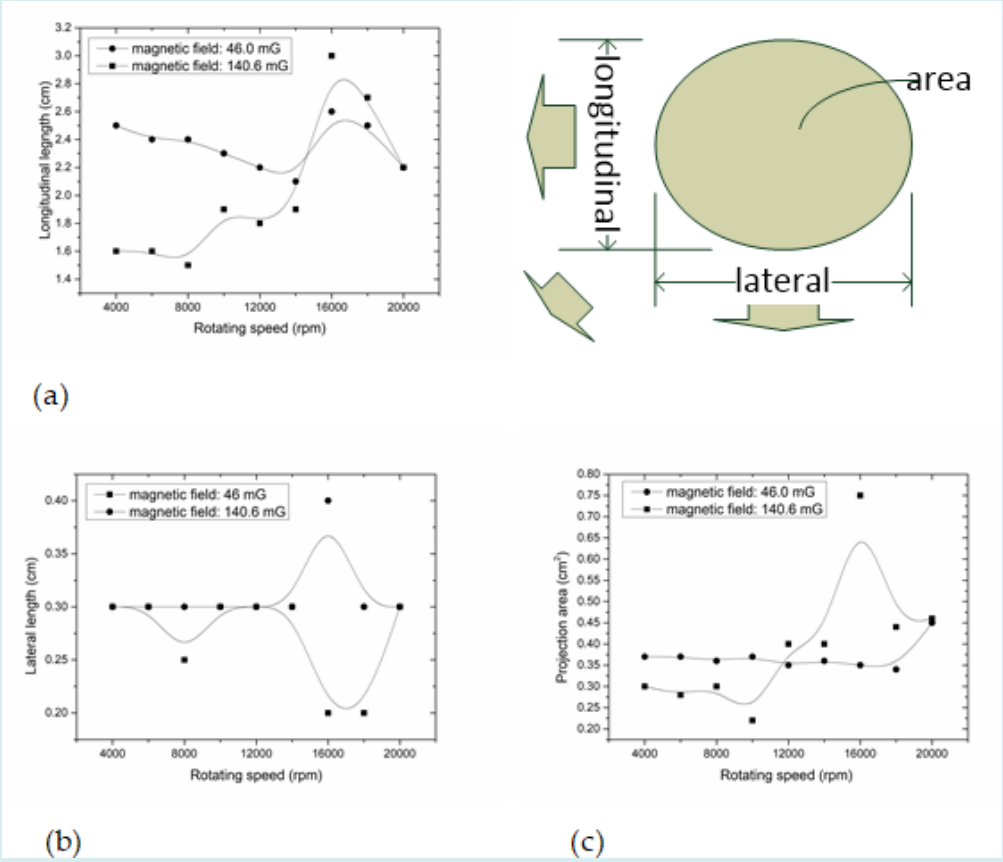

Figure 6: (a) Longitudinal length, (b) lateral length, and (c) stability of area as functions of rotation speed under different magnetic fields.

The longitudinal laser spots of the SPIONs are presented in Figure 6a. Under a low magnetic field of 46.0 mG, the nanoparticles exhibit local maximum stability at 14,000 rpm. However, under a high magnetic field of 140.6 mG, local maximum stability is observed at both 8,000 and 16,000 rpm. The lateral laser spots of these nanoparticles are presented

in Figure 6b. Under a low magnetic field of 46.0 mG, local maximum stability appears at 12,000 rpm, whereas under a high magnetic field of 140.6 mG, local maximum stabilities are observed at 8,000 rpm and between 16,000 and 18,000 rpm. Figure 6c presents the combined laser-spot areas of the SPIONs. Under a low magnetic field of 46.0 mG, these nanoparticles exhibit local maximum stability at 18,000 rpm. However, under a high magnetic field of 140.6 mG, more local maximum stabilities are apparent, specifically at 10,000 and 16,000 rpm. This behavior can be attributed to the high magnetic field from different magnets, under which a second local maximum stability occurs, exhibiting a higher dimensional value than that observed for the first one.

This issue can be explained using a simple equivalent circuit. At H = 46.0 mG for a ferromagnetic magnet, R0 = RInt represents the intrinsic resistance. At H = 140.6 mG for three ferromagnetic magnets, the cause R0 = RInt + RHet represents the resistance fluxes, where RInt is the first extreme intrinsic resistance and RHet is the second extreme heterogeneous resistance obtained from longitudinal and lateral lengths. RInt can be originally related to crystallinity, and RHet can be originally related to uniformity, as shown in Figure 7.

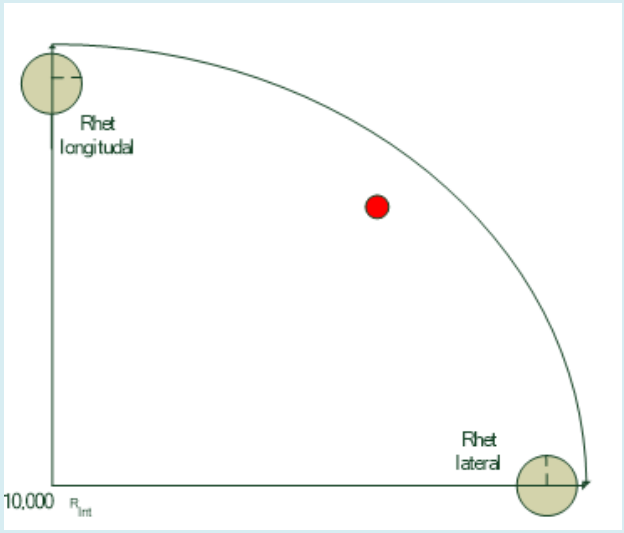

Figure 7: Intrinsic and heterogeneous equivalent polar coordinates R0.

Figure 8 illustrates the impact inversion recoveries of the SPIONs. Under a low magnetic field of 46 mG, these nanoparticles exhibit local stability at approximately 10,000 rpm. Similarly, under a high magnetic field of 140.6 mG, local stability is observed at 10,000 rpm. Both magnetic field intensities demonstrate the existence of local stability. This indicates that the nanoparticles have low energies at 10,000 rpm under both magnetic fields. This demonstration has low energies at 10,000 rpm at both magnetic fields.

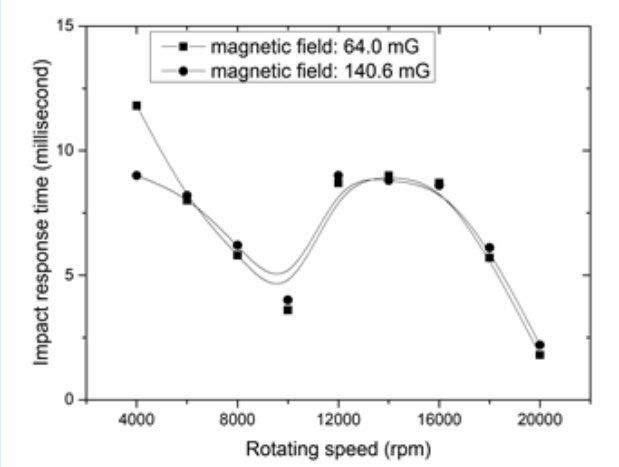

Figure 8: Impact response times relative to the rotation speed under different magnetic fields.

Conclusions

A sol–gel method was employed to form a nanoparticle film of the superparamagnetic material Fe_3O_4 via sputtering. The magnetization of this material increases with the increasing rotation speed when it acts as a rotating gyroscope. The maglev force exhibits a wide linear range. The size stability of the superparamagnetic nanoparticles also improve with the increasing rotation speed. Two stabilities observed for different magnets can reveal the nanoiron oxide used to dynamically measure crystallinity and uniformity. The inversion recovery of Fe_3O_4 reveals the same stabilization for superparamagnetic materials as Fe_3O_4.

References

1. Kim W, Trumper DL (1998) High-precision magnetic levitation stage for photolithography. Precis Eng 22(2): 66-77.

2. Mann BP, Sims ND (2009) Energy harvesting from the nonlinear oscillations of magnetic levitation. J Sound Vib 319(2): 515-530.

3. Bleuler H (1992) A survey of magnetic levitation and magnetic bearing types. JSME Int J 35(3): 335-342.

4. Hajjaji AE, Ouladsine M (2001) Modeling and nonlinear control of magnetic levitation systems. IEEE Trans Ind Electron 48(4): 831-838.

5. Al Muthairi NF, Zribi M (2004) Sliding mode control of a magnetic levitation system. Math Probl Eng 2: 93-107.

6. Ma KB, Postrekhin YV, Chu WK (2003) Superconductor and magnet levitation devices. Rev Sci Instrum 74(12): 4989-5017.

7. Sezer N, Arı I, Biçer Y, Koç M (2021) Superparamagnetic nanoarchitectures: multimodal functionalities and applications. J Magn Magn Mater 538: 168300.

8. Nisticò R (2021) A synthetic guide toward the tailored production of magnetic iron oxide nanoparticles. Bulle Soci Españ Cerámi Vidrio 60(1): 29-40.

9. Ashkarran AA, Gharibi H, Zeki DA, Radu I, Khalighinejad F, et al. (2022) Multi-omics analysis of magnetically levitated plasma biomolecules. Biosens Bioelectron 220: 114862.

10. Castro E, Mano JF (2013) Magnetic force-based tissue engineering and regenerative medicine. J Biomed Nanotechnol 9(7): 1129-1136.

11. Ashkarran AA, Suslick KS Mahmoudi M (2020) Magnetically levitated plasma proteins. Anal Chem 92(2): 1663-1668.